Theoretical Evaluation of the GNSS Synchronization Performance Degradation under Interferences

Conference Paper · September 2022

DOI: 10.33012/2022.18564

3 authors:

Lorenzo Ortega Espluga
Institut Polytechnique des Sciences Avancées

Jordi Vilà-Valls
Institut Supérieur de l'Aéronautique et de l'Espace (ISAE)

E. Chaumette
Institut Supérieur de l'Aéronautique et de l'Espace (ISAE)

Theoretical Evaluation of the GNSS Synchronization Performance Degradation under Interferences

Lorenzo Ortega, *IPSA, Toulouse, France*
Jordi Vilà-Valls, Eric Chaumette, *ISAE-Supaero, Toulouse, France*

BIOGRAPHY

Lorenzo Ortega is Associate Profesor at Institut Polytechnique des Sciences Avancées (IPSA), Toulouse, France. He received the MS in Electrical Engineering from Zaragoza University, Spain, in 2016 and PhD in Signal Processing from National Polytechnic Institute of Toulouse (INPT) in 2019. From 2020 to 2021, he was a postdoctoral researcher at the Institut Supérieur de l'Aéronautique et de l'Espace (ISAE-SUPAERO), University of Toulouse, France. His primary areas of interest include statistical signal processing, machine learning, estimation and detection theory, channel coding and digital communications, with applications to satellite communication, localization, tracking, navigation and remote sensing.

Jordi Vilà-Valls is Professor at the Institut Supérieur de l'Aéronautique et de l'Espace (ISAE-SUPAERO), University of Toulouse, France. He received the MS in Electrical Engineering from both Universitat Politècnica de Catalunya (UPC), Spain, and Grenoble Institute of Technology (INPG), France, in 2006, and the PhD in Signal Processing from INPG in 2010. His primary areas of interest include statistical signal processing, estimation and detection theory, nonlinear Bayesian inference and robust filtering, with applications to localization, tracking, navigation and remote sensing.

Eric Chaumette was born in 1965 at Chartres (France). He studied Electronics and Signal Processing both at ENAC (Toulouse, France) where he obtained an Engineer degree in 1989, and at Toulouse University where he obtained a M.Sc. degree in Signal Processing in 1989. From 1990 to 2007, he was with Thales in various radar studies departments. From 2007 to 2013, he was with the Electromagnetic and Radar Division of the French Aerospace Lab (ONERA), Palaiseau, France, as a research engineer. Simultaneously, from 2000 to 2014, he was a research associate at laboratory SATIE, CNRS, École Normale Supérieure de Cachan, France, where he received the PhD degree in 2004 and the "habilitation à diriger les recherches" in 2014. He is currently Professor at the Department of Electronics, Optronics and Signal of ISAE-SUPAERO, Toulouse, France. Main domains of interest are related to detection and estimation theory applied to localisation and navigation (GNSS, robust multi-sensor data fusion).

ABSTRACT

Global Navigation Satellite Systems (GNSS) are a key player in a plethora of applications, ranging from navigation and timing, to Earth observation or space weather characterization. For navigation purposes, interference scenarios are among the most challenging operation conditions, which clearly impact the maximum likelihood estimates (MLE) of the signal synchronization parameters. While several interference mitigation techniques exist, a theoretical analysis on the GNSS MLE performance degradation under interference, being fundamental for system/receiver design, is a missing tool. The main goal of this contribution is to provide such analysis, by deriving closed-form expressions of the estimation bias, for a generic GNSS signal corrupted by an interference. The proposed bias are validated for a tone interference and a linear frequency modulation chirp interference.

I. INTRODUCTION

Reliable position, navigation and timing information is fundamental in new application such as Intelligent Transportation Systems (ITS), automated aircraft landing or autonomous unmanned ground/air vehicles. In such applications, the main source of positioning information are Global Navigation Satellite Systems (GNSS) Teunissen and Montenbruck (2017), a technology which has attracted a lot of interest in the past decades. But GNSS were originally designed to operate in clear sky nominal conditions, and their performance clearly degrades under harsh environments. Among the non-nominal operation conditions, multipath, jamming (i.e., intentional or unintentional) and spoofing are the most challenging ones, being a key issue in safety-critical applications Amin et al. (2016). These interferences degrade GNSS performance, and can lead to denial of service or even counterfeit transmissions to control the receiver positioning solution. These effects have been reported in the state-of-the-art, and several interference mitigation countermeasures have been already proposed at different stages of the receiver Amin et al. (2017); Arribas et al. (2019); Borio and Gioia (2021); Fernández-Prades et al. (2016); Morales-Ferre et al. (2020). However, even with such a large pool of methods, a theoretical synchronization performance characterization under such conditions does not exist in the literature, and this is fundamental for receiver design and analysis.

From an estimation point of view, such performance characterization implies to theoretically analyze how different interferences degrade the acquisition and tracking stages (i.e., both being particular instances of the optimal maximum likelihood (ML) solution) of the GNSS receiver, and in turn the final position estimate. Because the optimal solution is given by the ML estimator, it is sound to obtain the corresponding Cramér-Rao bound (CRB), which provides a lower bound on the estimation performance of any (locally) unbiased estimator Trees and Bell (2007). Even if the CRBs for different GNSS receiver architectures operating under nominal conditions are available in the literature Das et al. (2020); Lubeigt et al. (2020); Medina et al. (2020); Medina et al. (2021); Ortega et al. (2022), such performance bounds have not been studied for the interference case of interest in this contribution. Indeed, performance bounds can provide precious information for the design of new GNSS signals, or for the design of next-generation interference countermeasures, therefore being an important missing point.

Preliminary work has empirically evidenced that interferences induce a bias on the parameter estimation. The main objective of the article is to provide the theoretical analysis of the effect of interferences on the GNSS receiver performance, i.e., how the GNSS synchronization (time-delay, Doppler and signal phase estimation) is degraded when the receiver is corrupted by an interfering signal. The main hypothesis is that the receiver does not have any countermeasure mechanism against such interferences. In other words, the GNSS receiver assumes that the received signal is only corrupted by additive noise, as in a standard operation regime. This implies that the signal model at the receiver input and the assumed signal model do not coincide, that is, there exists a model mismatch. In order to perform the analytical study of the estimation performance limits under model mismatch we resort to the theoretical computation of the bias induced by the interference. Notice that because the estimator is no longer unbiased, the mean square error (MSE) is the addition of the CRB and the squared bias, the latter being dominant for large interference powers. Then, the main challenge is to analytically compute the bias for a set of representative interferences that may corrupt the GNSS system.

The corresponding theoretical derivations and results are obtained for the following set of interferences: 1) single tone interference at the maximum spectral support; 2) single tone interference at first information lobe; 3) chirp interference centered at the maximum spectral support; and 4) chirp interference not centered at the maximum spectral support. Notice that once an analytical form is derived, this information can be used for: i) the derivation of metrics that allow to compare the robustness to interference of different GNSS signals, as well as for the design of new GNSS signals; ii) the design of next-generation interference countermeasures, e.g., robust estimation methods. In addition, in terms of estimation performance degradation the analysis provided in this article allows to assess, for instance, which is the maximum acceptable signal to noise+jammer power ratio for a correct receiver operation, or the expected synchronization performance under different jammer powers. A set of simulation results are provided to support the discussion and validate the theoretical derivations.

II. SIGNAL MODEL

1. Correctly Specified Signal Model

A GNSS band-limited signal $s(t)$, with bandwidth B, transmitted over a carrier frequency f_c ($\lambda_c = c/f_c$) is considered in this study. The complex analytical signal model is considered to be narrowband Dogandzic and Nehorai (2001), resulting in a negligible influence of the Doppler parameter on the signal samples. For short observation times, a good approximation of the baseband output of the receiver's Hilbert filter (GNSS signal + interference) is Skolnik (1990),

$$x(t;\boldsymbol{\eta}) = \alpha s\left(t-\tau\right) e^{-j2\pi f_c (b(t-\tau))} + I(t) + n\left(t\right), \tag{1}$$

with $\boldsymbol{\eta} = (\tau, b)^\top$, containing both the delay and Doppler shift, $f \in \left[-\frac{F_s}{2}, \frac{F_s}{2}\right]$, $I(t)$ an unknown interference, $n(t)$ a complex white Gaussian noise within F_s with unknown variance σ_n^2 and α a complex gain. The discrete vector signal model is built from $N = N_1 + N_2 + 1$ samples at $T_s = 1/F_s$,

$$\mathbf{x} = \alpha \mathbf{a}(\boldsymbol{\eta}) + \mathbf{n} = \rho e^{j\Phi} \mathbf{a}(\boldsymbol{\eta}) + \mathbf{n} = \alpha \boldsymbol{\mu}(\boldsymbol{\eta}) + \mathbf{I} + \mathbf{n}, \tag{2}$$

with $\mathbf{x} = \left(\ldots, x\left(kT_s\right), \ldots\right)^\top$, $\mathbf{I} = \left(\ldots, I\left(kT_s\right), \ldots\right)^\top$, $\mathbf{n} = \left(\ldots, n\left(kT_s\right), \ldots\right)^\top$, $N_1 \leq k \leq N_2$ signal samples, and

$$\mathbf{a}(\boldsymbol{\eta}) = (\ldots, s(kT_s - \tau)e^{-j2\pi f_c (b(kT_s - \tau)} + \frac{1}{\alpha} I(kT_s). \ldots)^\top, \tag{3}$$

$$\boldsymbol{\mu}(\boldsymbol{\eta}) = (\ldots, s(kT_s - \tau)e^{-j2\pi f_c (b(kT_s - \tau)} \ldots)^\top. \tag{4}$$

The unknown deterministic parameters can be gathered in vector $\boldsymbol{\epsilon}^\top = \left(\sigma_n^2, \rho, \Phi, \boldsymbol{\eta}^\top\right) = \left(\sigma_n^2, \boldsymbol{\theta}^\top\right)$, with $\rho \in \mathbb{R}^+, 0 \leq \Phi \leq 2\pi$. The correctly specified signal model is represented by a probability densitiy function (pdf) denoted $p_{\boldsymbol{\epsilon}}(\mathbf{x}; \boldsymbol{\epsilon})$, which follows a complex circular Gaussian distribution $\mathbf{x} \sim \mathcal{CN}(\alpha \mathbf{a}(\boldsymbol{\eta}), \sigma_n^2 \boldsymbol{I}_N)$.

2. Misspecified Signal Model

The misspecified signal model represents the case where the interference is not considered, i.e., when a mismatched ML estimator (MMLE) is implemented at the receiver. This nominal case leads to the definition of the misspecified parameter vector $\boldsymbol{\eta}' = [\tau', b']^\top$, and the complete set of unknown parameters $\boldsymbol{\epsilon'}^\top = \left[\sigma_n^2, \rho', \Phi', \boldsymbol{\eta}'^\top\right] = \left[\sigma_n^2, \boldsymbol{\theta}'^\top\right]$, yielding the following signal model at the output of the Hilbert filter,

$$x'(t; \boldsymbol{\eta}') = \alpha' s(t - \tau') e^{-j2\pi f_c b'(t-\tau')} + n(t) \tag{5}$$

with $\alpha' = \rho' e^{j\Phi'}$. Again, we can build the discrete vector signal model from $N = N_1 + N_2 + 1$ samples at $T_s = 1/F_s$,

$$\mathbf{x}' = \alpha' \boldsymbol{\mu}(\boldsymbol{\eta}') + \mathbf{n} \tag{6}$$

$$\boldsymbol{\mu}(\boldsymbol{\eta}') = (\ldots, s(kT_s - \tau') e^{-j2\pi f_c (b'(kT_s - \tau'))}, \ldots)^\top.$$

The misspecified signal model is represented by a pdf denoted $f_{\boldsymbol{\epsilon}'}(\mathbf{x}'; \boldsymbol{\epsilon}')$ which follows a complex circular Gaussian distribution $\mathbf{x}' \sim \mathcal{CN}(\alpha' \boldsymbol{\mu}(\boldsymbol{\eta}'), \sigma_n^2 \boldsymbol{I}_N)$. Note that under this particular scenario, the covariance matrix of the correctly specified signal model is equals the covariance matrix of the misspecified signal model, i.e. $\sigma_n^2 \boldsymbol{I}_N$ and this covariance matrix does not depend on the synchronization parameters of interest, then

$$p_{\boldsymbol{\epsilon}}(\mathbf{x}; \boldsymbol{\epsilon}) = \frac{1}{\pi^N \sigma_n^{2N}} e^{\frac{-(\mathbf{x} - \alpha \boldsymbol{a}(\boldsymbol{\eta}))^H (\mathbf{x} - \alpha \boldsymbol{a}(\boldsymbol{\eta}))}{\sigma_n^2}}, \quad f_{\boldsymbol{\epsilon}'}(\mathbf{x}'; \boldsymbol{\epsilon}') = \frac{1}{\pi^N \sigma_n^{2N}} e^{\frac{-(\mathbf{x} - \alpha' \boldsymbol{\mu}(\boldsymbol{\eta}'))^H (\mathbf{x} - \alpha' \boldsymbol{\mu}(\boldsymbol{\eta}'))}{\sigma_n^2}}. \tag{7}$$

When we consider a misspecified model and the corresponding MMLE, the estimation of the parameters of interest is biased. Those biased estimated parameters are commonly referred to as pseudo-true parameters. We denote them as $\boldsymbol{\theta}_{pt}^\top = [\rho_{pt}, \Phi_{pt}, \tau_{pt}, b_{pt}]$.

III. MISSPECIFIED SIGNAL MODEL: KULLBACK-LEIBLER DIVERGENCE

The pseudo-true parameters are simply those that give the minimum Kullback-Leibler (KLD) Divergence $D(p_{\boldsymbol{\epsilon}} || f_{\boldsymbol{\epsilon}'})$ between the true and assumed models (i.e., because the estimation is independent of σ_n^2),

$$D(p_{\boldsymbol{\epsilon}} || f_{\boldsymbol{\epsilon}'}) = E_p \left[\ln p_{\boldsymbol{\epsilon}}(\mathbf{x}; \boldsymbol{\epsilon}) - \ln f_{\boldsymbol{\epsilon}'}(\mathbf{x}; \boldsymbol{\epsilon}')\right], \tag{8}$$

$$\boldsymbol{\theta}_{pt} = \arg\min_{\boldsymbol{\theta}'} \left\{D(p_{\boldsymbol{\epsilon}} || f_{\boldsymbol{\epsilon}'})\right\} = \arg\min_{\boldsymbol{\theta}'} \left\{E_p \left[-\ln f_{\boldsymbol{\epsilon}'}(\mathbf{x}; \boldsymbol{\epsilon}')\right]\right\}, \tag{9}$$

where $E_p[\cdot]$ is the expectation with respect to (w.r.t.) the true model's pdf, and

$$\begin{aligned} &E_p \left[-\ln f_{\boldsymbol{\epsilon}'}\right] = -N \ln(\pi) - 2N \ln(\sigma_n) \\ &+ \frac{1}{\sigma_n^2} E_p \left[(\mathbf{x} - \alpha \mathbf{a}(\boldsymbol{\eta}) + \alpha \mathbf{a}(\boldsymbol{\eta}) - \alpha' \boldsymbol{\mu}(\boldsymbol{\eta}'))^H (\mathbf{x} - \alpha \mathbf{a}(\boldsymbol{\eta}) + \alpha \mathbf{a}(\boldsymbol{\eta}) - \alpha' \boldsymbol{\mu}(\boldsymbol{\eta}'))\right]. \end{aligned} \tag{10}$$

To minimize (10) w.r.t. the argument $\boldsymbol{\theta}'$, the equation can be simplified as,

$$\begin{aligned} &\arg\min_{\boldsymbol{\theta}'} \left\{E_p \left[-\ln f_{\boldsymbol{\epsilon}'}(\mathbf{x}; \boldsymbol{\epsilon}')\right]\right\} \\ &= \arg\min_{\boldsymbol{\theta}'} \left\{ E_p \left[\begin{array}{c} (\mathbf{x} - \alpha \mathbf{a}(\boldsymbol{\eta}))^H (\mathbf{x} - \alpha \mathbf{a}(\boldsymbol{\eta})) \\ +(\mathbf{x} - \alpha \mathbf{a}(\boldsymbol{\eta}))^H (\alpha \mathbf{a}(\boldsymbol{\eta}) - \alpha' \boldsymbol{\mu}(\boldsymbol{\eta}')) \\ +(\alpha \mathbf{a}(\boldsymbol{\eta}) - \alpha' \boldsymbol{\mu}(\boldsymbol{\eta}'))^H (\mathbf{x} - \alpha \mathbf{a}(\boldsymbol{\eta})) \\ +(\alpha \mathbf{a}(\boldsymbol{\eta}) - \alpha' \boldsymbol{\mu}(\boldsymbol{\eta}'))^H (\alpha \mathbf{a}(\boldsymbol{\eta}) - \alpha' \boldsymbol{\mu}(\boldsymbol{\eta}')) \end{array} \right] \right\} \\ &= \arg\min_{\boldsymbol{\theta}'} \left\{(\alpha \mathbf{a}(\boldsymbol{\eta}) - \alpha' \boldsymbol{\mu}(\boldsymbol{\eta}'))^H (\alpha \mathbf{a}(\boldsymbol{\eta}) - \alpha' \boldsymbol{\mu}(\boldsymbol{\eta}'))\right\} \\ &= \arg\min_{\boldsymbol{\theta}'} \left\{\|\alpha \mathbf{a}(\boldsymbol{\eta}) - \alpha' \boldsymbol{\mu}(\boldsymbol{\eta}')\|^2\right\}. \end{aligned}$$

We define the orthogonal projector $\Pi_{\mathbf{A}}^{\perp} = \mathbf{I} - \Pi_{\mathbf{A}}$ with $\Pi_{\mathbf{A}} = \mathbf{A}\left(\mathbf{A}^H\mathbf{A}\right)^{-1}\mathbf{A}^H$, which leads to

$$
\begin{aligned}
\|\alpha \mathbf{a}(\boldsymbol{\eta}) - \alpha' \boldsymbol{\mu}(\boldsymbol{\eta}')\|^2 &= \left\|\left(\Pi_{\boldsymbol{\mu}(\boldsymbol{\eta}'))} + \Pi^{\perp}_{\boldsymbol{\mu}(\boldsymbol{\eta}'))}\right)(\alpha \mathbf{a}(\boldsymbol{\eta}) - \alpha' \boldsymbol{\mu}(\boldsymbol{\eta}')))\right\|^2 \\
&= \left\|\Pi_{\boldsymbol{\mu}(\boldsymbol{\eta}'))}(\alpha \boldsymbol{a}(\boldsymbol{\eta}) - \alpha' \boldsymbol{\mu}(\boldsymbol{\eta}'))\right\|^2 + \left\|\Pi^{\perp}_{\boldsymbol{\mu}(\boldsymbol{\eta}')}(\alpha \boldsymbol{a}(\boldsymbol{\eta}) - \alpha' \boldsymbol{\mu}(\boldsymbol{\eta}'))\right\|^2 \\
&= \left\|\Pi_{\boldsymbol{\mu}(\boldsymbol{\eta}')}\alpha \boldsymbol{a}(\boldsymbol{\eta}) - \alpha' \boldsymbol{\mu}(\boldsymbol{\eta}')\right\|^2 + \left\|\Pi^{\perp}_{\boldsymbol{\mu}(\boldsymbol{\eta}')}\alpha \boldsymbol{a}(\boldsymbol{\eta})\right\|^2 \\
&= \left\|\boldsymbol{\mu}(\boldsymbol{\eta}')\left(\frac{\boldsymbol{\mu}(\boldsymbol{\eta}')^H \alpha \boldsymbol{a}(\boldsymbol{\eta})}{\boldsymbol{\mu}(\boldsymbol{\eta}')^H \boldsymbol{\mu}(\boldsymbol{\eta}')} - \alpha'\right)\right\|^2 + \|\alpha \boldsymbol{a}(\boldsymbol{\eta})\|^2 - \left\|\Pi_{\boldsymbol{\mu}(\boldsymbol{\eta}')}\alpha \boldsymbol{a}(\boldsymbol{\eta})\right\|^2,
\end{aligned}
$$

then the parameters that minimize the KLD are,

$$
\arg\min_{\boldsymbol{\theta}'}\left\{\|\alpha \boldsymbol{a}(\boldsymbol{\eta}) - \alpha' \boldsymbol{\mu}(\boldsymbol{\eta}')\|^2\right\} \Leftrightarrow \begin{cases} \alpha_{pt} = \alpha \frac{\boldsymbol{\mu}(\boldsymbol{\eta}_{pt})^H \boldsymbol{a}(\boldsymbol{\eta})}{\boldsymbol{\mu}(\boldsymbol{\eta}_{pt})^H \boldsymbol{\mu}(\boldsymbol{\eta}_{pt})} \\ \boldsymbol{\eta}_{pt} = \arg\max_{\boldsymbol{\eta}'}\left\{\left\|\Pi_{\boldsymbol{\mu}(\boldsymbol{\eta}')}\alpha \boldsymbol{a}(\boldsymbol{\eta})\right\|^2\right\} \end{cases}
$$

with $\alpha_{pt} = \rho_{pt} e^{j\Phi_{pt}}$ and $\boldsymbol{\eta}_{pt}^{\top} = [\tau_{pt}, b_{pt}]$. This result may be connected with the asymptotic behavior of the MMLE,

$$
\begin{cases} \widehat{\alpha} = \frac{\boldsymbol{\mu}(\widehat{\boldsymbol{\eta}})^H \mathbf{x}}{\boldsymbol{\mu}(\widehat{\boldsymbol{\eta}})^H \boldsymbol{\mu}(\widehat{\boldsymbol{\eta}})} \\ \widehat{\boldsymbol{\eta}} = \arg\max_{\boldsymbol{\eta}'}\left\{\left\|\Pi_{\boldsymbol{\mu}(\boldsymbol{\eta}')}\mathbf{x}\right\|^2\right\} \end{cases} \underset{SNR\to\infty}{\overrightarrow{\quad}} \begin{cases} \widehat{\alpha} = \alpha \frac{\boldsymbol{\mu}(\widehat{\boldsymbol{\eta}})^H \boldsymbol{a}(\boldsymbol{\eta})}{\boldsymbol{\mu}(\widehat{\boldsymbol{\eta}})^H \boldsymbol{\mu}(\widehat{\boldsymbol{\eta}})} = \alpha_{pt} \\ \widehat{\boldsymbol{\eta}} = \arg\max_{\boldsymbol{\eta}'}\left\{\left\|\Pi_{\boldsymbol{\mu}(\boldsymbol{\eta}')}\alpha \boldsymbol{a}(\boldsymbol{\eta})\right\|^2\right\} = \boldsymbol{\eta}_{pt} \end{cases} \tag{11}
$$

Because the pseudo-true parameters are those that give the minimum KLD between the true and assumed models, which can be obtained by computing the MMLE without noise, we can define the bias as,

$$
\Delta\alpha = \alpha_{pt} - \alpha, \quad \boldsymbol{\Delta\eta} = \boldsymbol{\eta}_{pt} - \boldsymbol{\eta}. \tag{12}
$$

IV. BIAS COMPUTATION AND RESULTS FOR WELL-KNOWN INTERFERENCE MODELS

1. Preliminaries

Hereafter we further study (11) for the time-delay and Doppler bias calculation. Notice that,

$$
\left\|\Pi_{\boldsymbol{\mu}(\boldsymbol{\eta}')}\alpha \boldsymbol{a}(\boldsymbol{\eta})\right\|^2 = \alpha^2 \boldsymbol{a}(\boldsymbol{\eta})^H \Pi_{\boldsymbol{\mu}(\boldsymbol{\eta}')}\boldsymbol{a}(\boldsymbol{\eta}) = \alpha^2 \boldsymbol{a}(\boldsymbol{\eta})^H \boldsymbol{\mu}(\boldsymbol{\eta}')\left(\boldsymbol{\mu}(\boldsymbol{\eta}')^H \boldsymbol{\mu}(\boldsymbol{\eta}')\right)^{-1}\boldsymbol{\mu}(\boldsymbol{\eta}')^H \boldsymbol{a}(\boldsymbol{\eta}), \tag{13}
$$

with $\left(\boldsymbol{\mu}(\boldsymbol{\eta}')^H \boldsymbol{\mu}(\boldsymbol{\eta}')\right)^{-1} = 1/(F_s E_c)$ and E_c the chip energy (usually normalized to 1). Then,

$$
\left\|\Pi_{\boldsymbol{\mu}(\boldsymbol{\eta}')}\alpha \boldsymbol{a}(\boldsymbol{\eta})\right\|^2 = \frac{\alpha^2}{F_s E_c}\left|\boldsymbol{\mu}(\boldsymbol{\eta}')^H \boldsymbol{a}(\boldsymbol{\eta})\right|^2 = \frac{\alpha^2 F_s}{E_c}\left|\frac{\boldsymbol{\mu}(\boldsymbol{\eta}')^H \boldsymbol{a}(\boldsymbol{\eta})}{F_s}\right|^2 = \frac{\alpha^2 F_s}{E_c}\left|R_{\boldsymbol{a}(\boldsymbol{\eta}),\boldsymbol{\mu}(\boldsymbol{\eta}')}(\boldsymbol{\eta}')\right|^2, \tag{14}
$$

where $\frac{\boldsymbol{\mu}(\boldsymbol{\eta}')^H \boldsymbol{a}(\boldsymbol{\eta})}{F_s}$ is the cross-correlation function $R_{\boldsymbol{a}(\boldsymbol{\eta}),\boldsymbol{\mu}(\boldsymbol{\eta}')}(\boldsymbol{\eta}')$. In order to compute the bias of interest, we need to consider (i) the scenario with the unknown interference and (ii) set the noise equal to zero (refer to (11)). We can rewrite the previous equations as,

$$
\left\|\Pi_{\boldsymbol{\mu}(\boldsymbol{\eta}')}\alpha \boldsymbol{a}(\boldsymbol{\eta})\right\|^2 = \frac{F_s}{E_c}\left|\frac{\boldsymbol{\mu}(\boldsymbol{\eta}')^H \alpha \boldsymbol{\mu}(\boldsymbol{\eta})}{F_s} + \frac{\boldsymbol{\mu}(\boldsymbol{\eta}')^H \boldsymbol{I}}{F_s}\right|^2 = \frac{F_s}{E_c}\left|\alpha R_{\boldsymbol{\mu}(\boldsymbol{\eta}'),\boldsymbol{\mu}(\boldsymbol{\eta}')}(\boldsymbol{\eta}') + R_{\boldsymbol{I},\boldsymbol{\mu}(\boldsymbol{\eta}')}(\boldsymbol{\eta}')\right|^2. \tag{15}
$$

with $\boldsymbol{I} = I(\cdots, kT_s, \cdots)$ the interference samples. It is important to notice that a bias appears if the correlation function $R_{\boldsymbol{I},\boldsymbol{\mu}(\boldsymbol{\eta}')}(\boldsymbol{\eta}')$ shifts in time-delay or Doppler the maximum value of the correlation function $R_{\boldsymbol{\mu}(\boldsymbol{\eta}'),\boldsymbol{\mu}(\boldsymbol{\eta}')}(\boldsymbol{\eta}')$.

In the following we consider the bias for GPS C/A signals. These signals are generated by concatenating pseudo-random noise (PRN) codes, which have good autocorrelation properties.

2. One Tone Interference at the Maximum Spectral Support

Let us consider the case where a jammer is generating a tone where most of the information is being transmitted, i.e., at the maximum spectral support. In the case of the GPS C/A signal, the maximum energy is transmitted at the carrier frequency, since GPS C/A uses a binary phase shift keying (BPSK) modulation. Then, after the Hilbert filter the tone is located at the baseband frequency, i.e., at frequency 0, which involves that the interference is a constant signal with amplitude A_i. For this particular case,

$$R_{\boldsymbol{I},\boldsymbol{\mu}(\boldsymbol{\eta}')}(\tau') = A_i \sum_{k=1}^{1023} C_{l,k}, \tag{16}$$

that is, a constant value. $C_{l,k}$ are the discrete values of the PRN code. Index l refers to the PRN code and index k refers to the chip value. For balanced Gold codes, $\sum_{k=1}^{1023} C_{l,k} = -1$. Because the interference-related term is constant,

$$\arg\max_{\tau'} \left| R_{\boldsymbol{\mu}(\tau'),\boldsymbol{\mu}(\tau')}(\tau) + R_{\boldsymbol{I},\boldsymbol{\mu}(\tau')}(\tau) \right|^2 = \arg\max_{\tau} \left| R_{\boldsymbol{\mu}(\tau'),\boldsymbol{\mu}(\tau')}(\tau) \right|^2, \tag{17}$$

and there is no bias induced by such interference. So in terms of jamming capabilities, it is not a good idea for the jammer to introduce a tone at the maximum spectral support.

Notice that this particular case is not realistic since the receiver performs the correlation operation with a signal limited in time, i.e., the interference tone should be multiplied by a rectangular window. Therefore, at the receiver, the interference should be modeled by a cardinal sine centered at the tone frequency. The width of the cardinal sine depends on the duration of the received signal. Because the cardinal sine will be centered at frequency 0, a large amount of power is required in order to damage the time-delay estimation. In contrast, the Doppler estimation is impacted by such interference. These effects are shown in Figures 1 and 2, where we provide the empirical MSE together with the theoretical CRB and bias for different scenarios:

- Figure 1: time-delay MSE and CRB. In blue, fixed jammer amplitude and three values for the jammer phase. In red, fixed jammer phase and three different jammer amplitudes.
- Figure 2 (left plot): Doppler MSE, CRB and bias, fixed jammer amplitude $A_i = 10$, and three values of jammer phase.
- Figure 2 (right plot): Doppler MSE, CRB and bias, fixed jammer phase $\phi = 0$, and three values of jammer amplitude.

In all the scenarios considered, the jammer is at $f_i = 0$, the signal has a Doppler of 500 Hz, and the receiver considers a 2 ms integration time. SNR$_{out}$ refers to the signal-to-noise ratio at the output of the ML matched filter. It is imporant to notice that when the jammer power is too large, the receiver front-end is saturated and therefore not able to demodulate any kind of signal.

Regarding the results, as already anticipated, a single tone jammer (for the set of tested amplitude and phase values) has no impact on the time-delay estimation performance. For the Doppler estimation, in contrast, a bias is induced on the MMLE. Notice that both different jammer phases and amplitudes lead to different results. For instance, for a fixed amplitude, an in-phase jammer, $\phi = 0$, has no impact on the Doppler, and the larger bias is induced by the $\phi = \pi$ case. Obviously, for a fixed jammer phase (not equal to 0), a larger jammer amplitude induces a larger bias. Regardless of the performance degradation, these results show the validity of the theoretical derivations, given that the empirical MSE converges to the theoretical bias. Notice that in practice a standard receiver operates at a SNR$_{out}$ between 15 and 25 dB. Larger values only appear for extended integration schemes, where the impact of the interference is larger w.r.t. the optimal MSE (CRB).

3. One Tone Interference at First Information Lobe

Because a single tone at the maximum spectral support has no impact on the time-delay estimaton, in the sequel we consider that the tone is located at a frequency f_i such that $-F_c \leq f_i \leq F_c$ with F_c the modulation (BPSK) chip rate. For this particular case, the interference samples are given by $\boldsymbol{I} = I(\cdots, A_i e^{j2\pi f_i k T_s + j\phi}, \cdots)$, which is a complex function, and can be rewritten as,

$$\boldsymbol{I} = I(\cdots, A_i e^{j2\pi f_i k T_s + j\phi}, \cdots) = I(\cdots, A_i \left(\cos(2\pi f_i k T_s + \phi) + j \sin(2\pi f_i k T_s + \phi)\right), \cdots) \tag{18}$$

with ϕ the initial phase of the tone. The correlation function it is a periodic signal that depends on the tone frequency f_i. The bias induced by such interference depends on both ϕ and f_i. The corresponding results are shown in Figures 3 and 4, for the time-delay and Doppler estimation, respectively. In these results the tone is at $f_i = 0.5$ MHz.

Again, the asymptotic empirical MSE coincides with the theoretical bias. In contrast to the previous case, a single tone within the main BPSK lobe ($f_i \neq 0$) induces a bias on both time-delay and Doppler estimation.

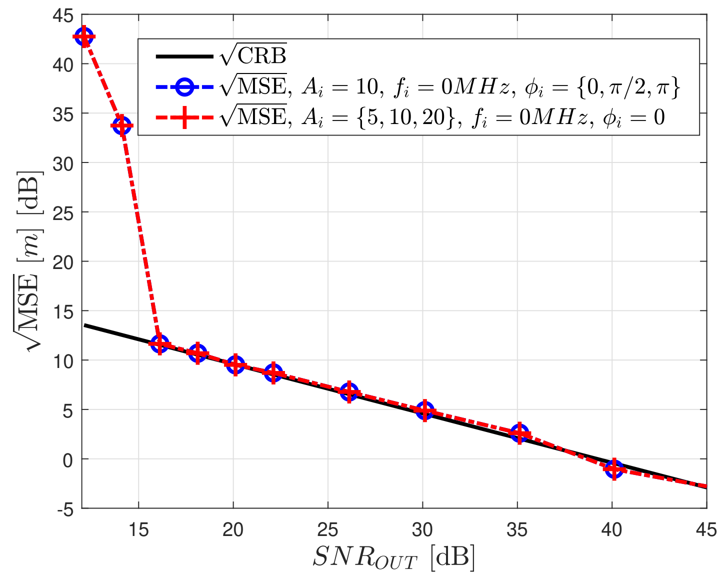

Figure 1: MSE for the time-delay estimation with a single tone jammer at $f_i = 0$.

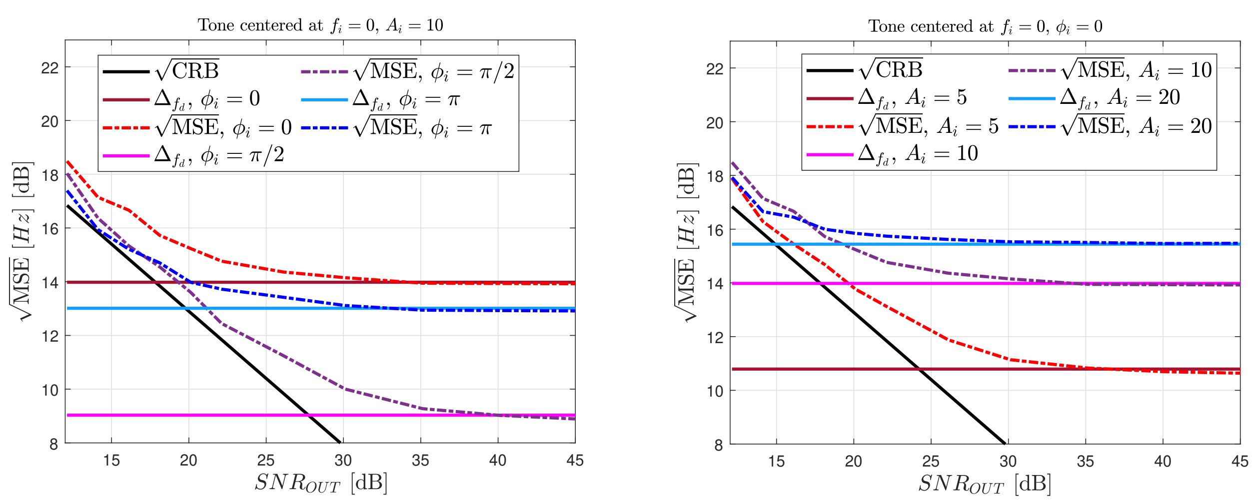

Figure 2: MSE and bias for the Doppler estimation with a single tone jammer at $f_i = 0$. Different jammer ϕ_i (left) and A_i (right).

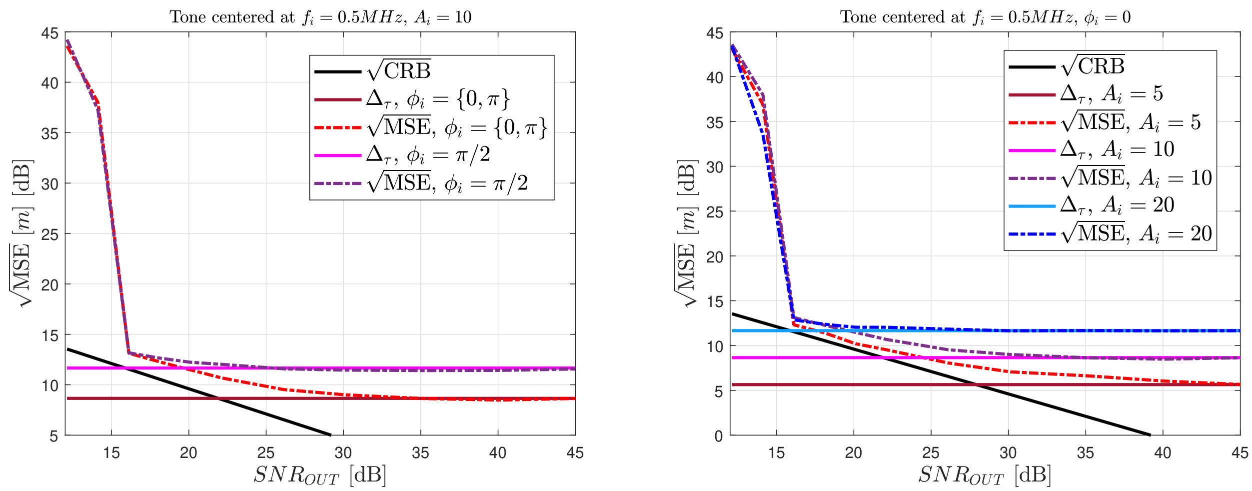

Figure 3: MSE and bias for the time-delay estimation with a single tone jammer at $f_i = 0.5$ MHz, for different jammer ϕ_i (left) and A_i (right).

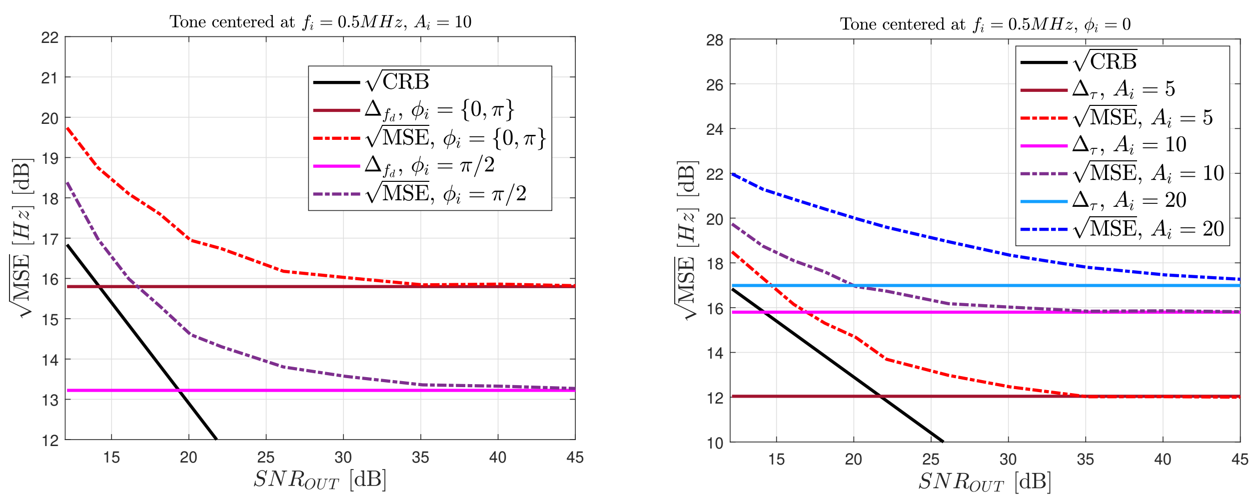

Figure 4: MSE and bias for the Doppler estimation with a single tone jammer at $f_i = 0.5$ MHz, for different jammer ϕ_i (left) and A_i (right).

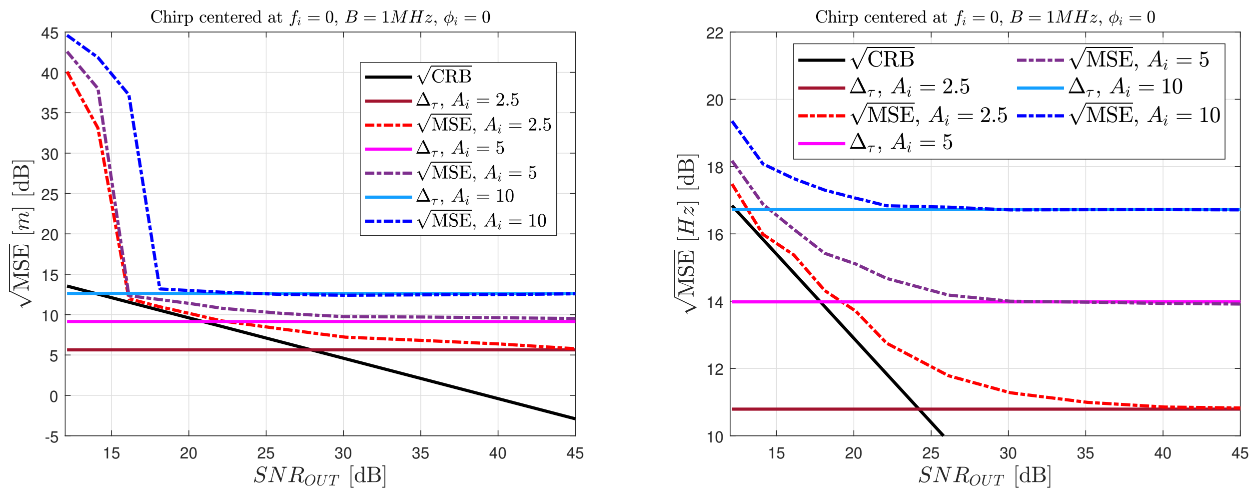

Figure 5: MSE and bias for the time-delay (left) and Doppler (right) estimation with a chirp centered at $f_i = 0$, for different jammer amplitudes A_i. Chirp bandwidth 1 MHz and initial jammer phase $\phi = 0$.

4. Chirp Interference in the First Lobe

The well-known linear frequency modulation (LFM) chirp signal is defined as,

$$\Phi(t) = \Pi_T(t) \times e^{j\pi\alpha t^2 + j\phi},\ \Pi_T(t) = \begin{cases} A_i & 0 \leq t < T \\ 0 & \text{otherwise} \end{cases} \tag{19}$$

with α the chirp rate and $T = NT_s$ the waveform period. The instantaneous frequency is $f(t) = \frac{1}{2\pi}\frac{d}{dt}\left(\pi\alpha t^2\right) = \alpha t$, and therefore the waveform bandwidth is $B = \alpha T$. To define a chirp centered at frequency $f_i = 0$, we can rewrite the chirp function as,

$$\Phi(t) = \Pi_T(t) \times e^{j\pi\alpha(t-T/2)^2 + j\phi},\ \Pi_T(t) = \begin{cases} A_i & 0 \leq t < T \\ 0 & \text{otherwise} \end{cases} \tag{20}$$

The MSE and bias results for a chirp bandwidth equal to 1 MHz and an initial jammer phase $\phi = \pi/2$ are shown in Figure 5. Compared to the previous single tone case, a chirp induces a larger bias on both time-delay and Doppler estimation. To further complete the analysis, the results for a chirp centered at $f_i = 0.5$ MHz are shown in Figure 6. It is interesting to notice that a non-centered chirp has less impact than a centered one.

V. CONCLUSIONS

It is well documented in the literature that interferences may have a huge impact on GNSS receivers' performance, but to the best of our knowledge the theoretical analysis of the impact of such intereferences on the first receiver stage was not available. In practice, there exists a model mismatch and interferences induce a bias. In this contribution, we performed the theoretical computation of the bias induced into the synchronization parameters ML estimates, that is, the performance degradation of the time-delay and Doppler estimation. This analysis was conducted for a set of representative single tone and chirp interferences, and results were provided for different scenarios to show the validity of the derivation and the possible impact on both time-delay and Doppler estimation. It is important to notice that such analysis may be the starting point for both the derivation of robustness metrics or new GNSS signals, and the design of interference countermeasures.

ACKNOWLEDGEMENTS

This work has been partially supported by the DGA/AID projects 2019.65.0068.00.470.75.01, 2021.65.0070.00.470.75.01, and TéSA.

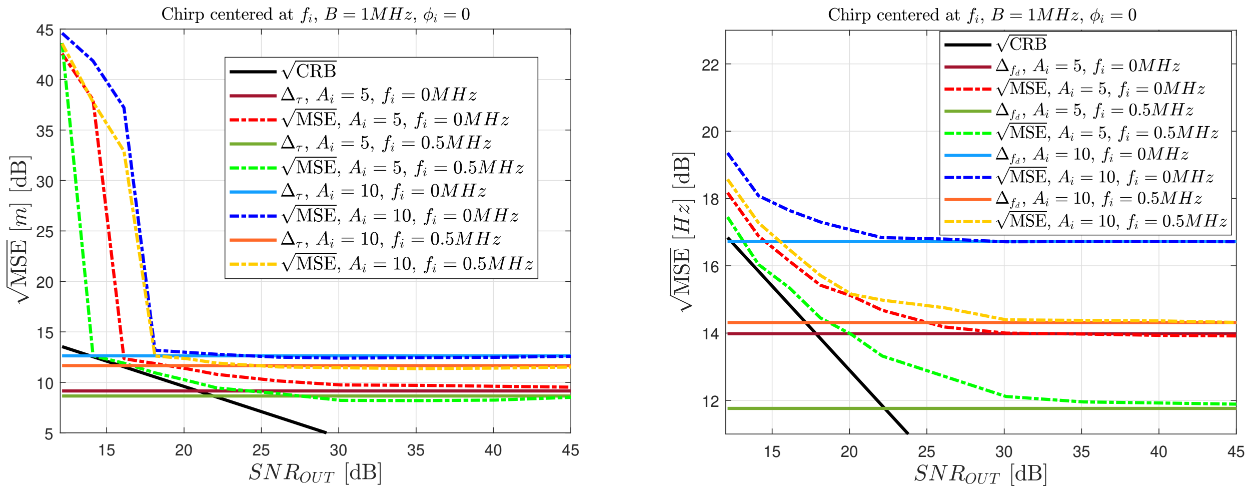

Figure 6: MSE and bias for the time-delay (left) and Doppler (right) estimation with a chirp centered at $f_i = 0$ and $f_i = 0.5$MHz, for different jammer amplitudes A_i. Chirp bandwidth 1 MHz and initial jammer phase $\phi = 0$.

REFERENCES

Amin, M. G., Borio, D., Zhang, Y. D., and Galleani, L. (2017). Time-Frequency Analysis for GNSSs: From Interference Mitigation to System Monitoring. *IEEE Signal Process. Mag.*, 34(5):85–95.

Amin, M. G., Closas, P., Broumandan, A., and Volakis, J. L. (2016). Vulnerabilities, Threats, and Authentication in Satellite-Based Navigation Systems [scanning the issue]. *Proceedings of the IEEE*, 104(6):1169–1173.

Arribas, J., Vilà-Valls, J., Ramos, A., Fernández-Prades, C., and Closas, P. (2019). Air Traffic Control Radar Interference in the Galileo E6 Band: Detection and Localization. *Navigation*, 66(3):505–522.

Borio, D. and Gioia, C. (2021). GNSS Interference Mitigation: A Measurement and Position Domain Assessment. *Navigation*, 68(1):93–114.

Das, P., Vilà-Valls, J., Vincent, F., Davain, L., and Chaumette, E. (2020). A New Compact Delay, Doppler Stretch and Phase Estimation CRB with a Band-Limited Signal for Generic Remote Sensing Applications. *Remote Sensing*, 12(18):2913.

Dogandzic, A. and Nehorai, A. (2001). Cramér-Rao Bounds for Estimating Range, Velocity, and Direction with an Active Array. *IEEE Trans. Signal Process.*, 49(6):1122–1137.

Fernández-Prades, C., Arribas, J., and Closas, P. (2016). Robust GNSS Receivers by Array Signal Processing: Theory and Implementation. *Proceedings of the IEEE*, 104(6):1207–1220.

Lubeigt, C., Ortega, L., Vilà-Valls, J., Lestarquit, L., and Chaumette, E. (2020). Joint Delay-Doppler Estimation Performance in a Dual Source Context. *Remote Sensing*, 12(23).

Medina, D., Ortega, L., Vilà-Valls, J., Closas, P., Vincent, F., and Chaumette, E. (2020). Compact CRB for Delay, Doppler and Phase Estimation - Application to GNSS SPP & RTK Performance Characterization. *IET Radar, Sonar & Navigation*, 14(10):1537–1549.

Medina, D., Vilà-Valls, J., Chaumette, E., Vincent, F., and Closas, P. (2021). Cramér-Rao Bound for a Mixture of Real- and Integer-Valued Parameter Vectors and its Application to the Linear Regression Model. *Signal Processing*, 179:107792.

Morales-Ferre, R., Richter, P., Falletti, E., de la Fuente, A., and Lohan, E. S. (2020). A Survey on Coping With Intentional Interference in Satellite Navigation for Manned and Unmanned Aircraft. *IEEE Commun. Surv. Tutor.*, 22(1):249–291.

Ortega, L., Vilà-Valls, J., and Chaumette, E. (2022). Insights on the estimation performance of gnss-r coherent and noncoherent processing schemes. *IEEE Geoscience and Remote Sensing Letters*, 19:1–5.

Skolnik, M. I. (1990). *Radar Handbook*. McGraw-Hill, New York, USA, 3rd edition.

Teunissen, P. J. G. and Montenbruck, O., editors (2017). *Handbook of Global Navigation Satellite Systems*. Springer, Switzerland.

Trees, H. L. V. and Bell, K. L., editors (2007). *Bayesian Bounds for Parameter Estimation and Nonlinear Filtering/Tracking*. Wiley/IEEE Press, NY, USA.